Proceedings of the SEM Annual Conference
June 7-10, 2010 Indianapolis, Indiana USA

Coupled Experimental and Computational Analysis of Fracture Path Selection in PMMA Blocks

C. L. Tsai[1], Y. L. Guan[1], R. C. Batra[1], D. C. Ohanehi[1], J. G. Dillard[2], E. Nicoli[1], D. A. Dillard[1],
[1]Department of Engineering Science and Mechanics
[2]Department of Chemistry
Virginia Polytechnic Institute and State University
Blacksburg, Virginia

Abstract

While developing experimental and computational tools for analyzing crack path selection and failure loci in adhesively bonded joints, we have initially applied these tools for studying crack paths in pre-notched monolithic blocks of polymethyl methacrylate (PMMA), a common material for conducting brittle fracture experiments. Specimen configurations similar to the compact tension specimen but of varying length/width ratios were used to explore the effect of the T-stress on destabilizing the crack from growing straight along its original direction. Asymmetric versions of this geometry were also used to determine the effect of imposed mode mixity on crack path selection. These test configurations provided useful data for checking the robustness of the computational software based on a meshless local Petrov-Galerkin formulation of the boundary-value problem. The PMMA was assumed to be linear elastic, homogeneous and isotropic. A crack was assumed to initiate when the maximum principal tensile stress reached a critical value and propagate in the direction of the eigenvector of this stress. Effects of the mode-mixity on the crack propagation have been studied.

Introduction

Crack trajectories in adhesive bonds and brittle materials under mixed-mode loading are of interest in applications in biomedical implant, microelectronic, transportation, and energy devices and machinery. PMMA (polymethyl methacrylate), a transparent polymer, is the material used in the current study on crack propagation. PMMA has been employed in numerous studies to observe crack trajectories [1-5] in a range of specimen geometries including semi-circular bend (SCB), four-point bend (FPB), Brazilian disc (BD), and diagonally loaded square plate (DLSP). The current work covers a first series of tests to explore crack trajectories under mixed-mode loading of monolithic PMMA specimens.

Using angled-cracked plate specimens, Smith et al. studied the mixed-mode fracture response of PMMA blocks (and brittle materials, in general) and explained crack trajectories in terms of the sign of the T-stress [3]. The T-stress, an important nonsingular term in Williams expansion[6] of stresses near a crack tip, is tangent to the crack, depends on the specimen geometry and loading conditions, and governs the stability of the growing crack. Aliha et al., using four specimen geometries, demonstrated the geometry dependence of the measured fracture toughness, and explained the dependence using the sign of the T-stress [1]. The mode mixity was varied from pure mode I to pure mode II through changes in the angle of the initial crack for various specimens, and the corresponding fracture toughness was computed. The crack trajectories for a series of SCB specimens were very instructive, showing a straight crack for pure mode I (initial crack inclination angle = 0^o) and ending with a crack kink for mode II (initial crack inclination angle = 50^o) [1].

For the current study, experiments were conducted on notched PMMA blocks that were similar to compact tension (CT) specimens, but had varying length/width ratios to explore effects of fracture mode mixity and the T-stress. The findings of these tests can provide an understanding of crack propagation in monolithic and isotropic materials and validate computational models being developed. For the numerical studies, the meshless local Petrov-Garlekin formulation of the boundary-value problem using the symmetric smoothed particle hydrodynamics (SSPH) basis functions for the trial solution was employed. Values of various parameters in the weight (or the test) function were optimized by studying the mode-I fracture problem for which analytical solution is known. Results of the computational studies were used to compute the stress concentration factor (SCF), the stress intensity factor (SIF), and the T-stress for simple tensile deformations of a square plate with a hole at the center.

T. Proulx (ed.), *Time Dependent Constitutive Behavior and Fracture/Failure Processes, Volume 3*, Conference Proceedings of the Society for Experimental Mechanics Series 15, DOI 10.1007/978-1-4419-9794-4_3, © The Society for Experimental Mechanics, Inc. 2011

The same software was used to analyze test configurations, and computed results were compared with the experimental findings. The software was also used to design experimental configurations that will give desired mode-mixity.

Experimental Study Using PMMA

Fracture tests were conducted on CT and modified CT specimens of 12.7 mm thick PMMA sheets. All tests were conducted on an Instron 5800R machine using a 5kN load cell. With one arm of the CT specimen fixed by the pin and the clevis, the other arm of the specimen was displaced downwards by the loading clevis.

CT Specimen Tests

A standard CT specimen (recommended in ASTM D 5045), shown in Fig. 1, has the thickness B=12.7mm (1/2''), w=25.4mm (1'') and a=12.7mm (0.5'') [7]. Tests on the CT specimens were conducted using a crosshead displacement rate of 10 mm/min, as recommended in ASTM D5045. To ensure consistency in K_{Ic} values for all the specimens, sharp initial cracks were necessary. The sharp initial cracks were produced by driving a wedge into the specimens. The initial cracks were made carefully with a razor blade and a wooden hammer after machining the notches. The blade and two shims were inserted in the notch to center the blade and to keep it parallel to the centroidal axis of the notch. Then, gentle hammer blows were applied to the back of the blade, initiating a tiny crack, only a few millimeters in front of the blade, and avoiding a large initial crack, propagating too far into the specimen. A picture of three specimens, prior to the tests, is shown in Fig. 2.

Relationships between the load and the crosshead displacement for three specimens are exhibited in Fig. 3. From these results, the average value of K_{Ic} was determined to be 1.056 ± 0.029 MPa$\sqrt{m}$. As expected, the crack trajectories remained straight.

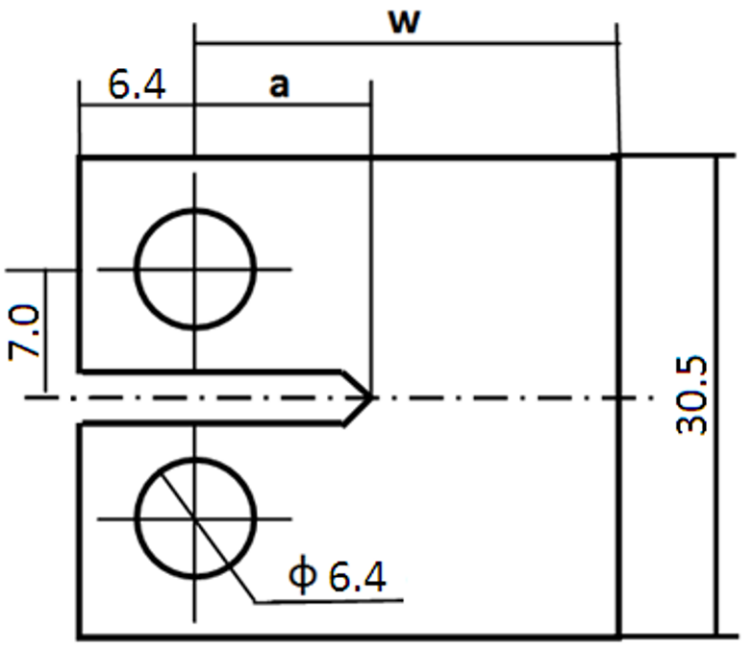

Fig. 1. PMMA CT Specimen with w=25.4mm (1'') and a=12.7mm (0.5''); B, specimen thickness = 12.7mm (0.5''). (All dimensions in mm).

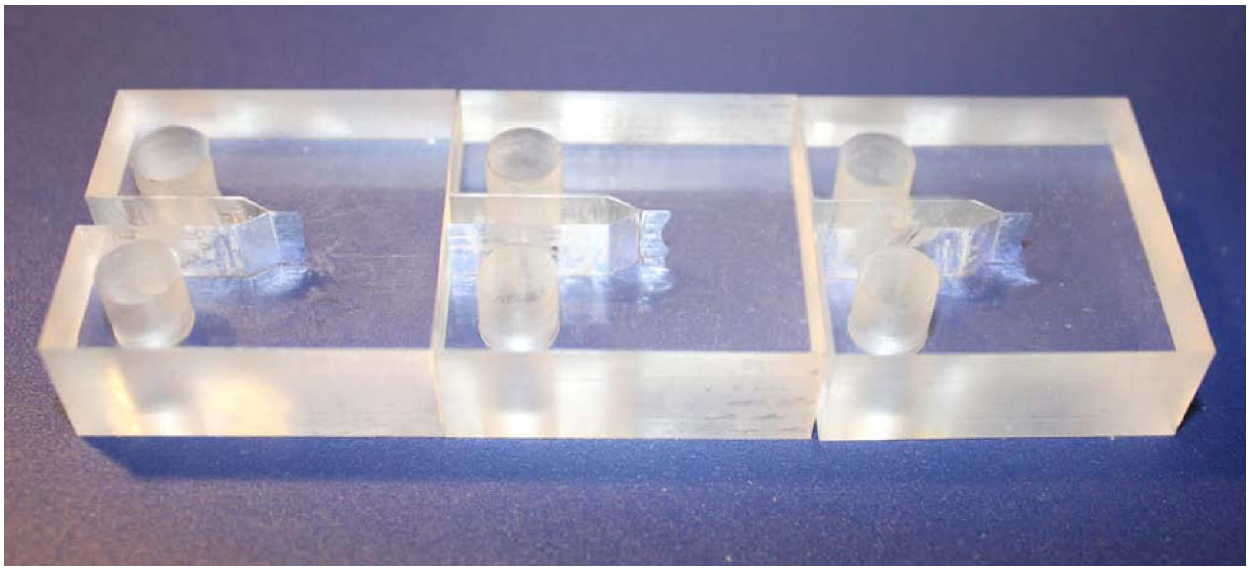

Fig. 2. Notches and Initial Cracks before the Tests.

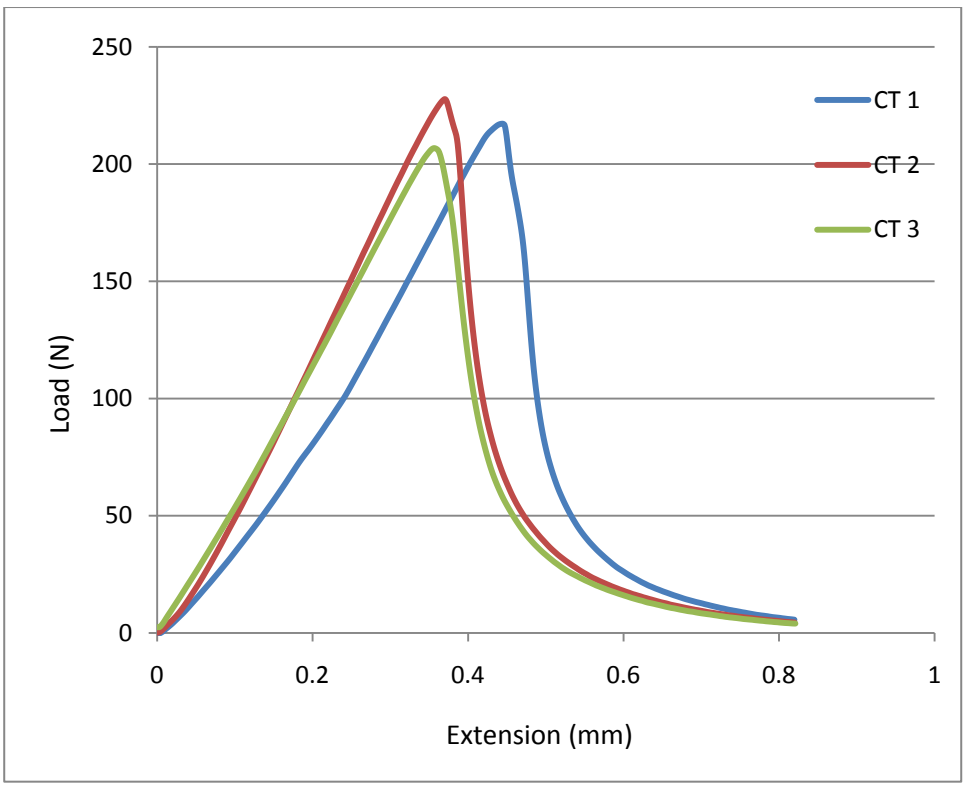

Fig. 3. Load-Extension Curves for the three CT specimens.

Effect of Notch Asymmetry on Crack Path Trajectory

Unlike specimens described above that had a notch placed along the horizontal centroidal axis, specimens with the notch and the starting crack not located along the horizontal centroidal axis("modified" or "asymmetric" CT

specimens) were also tested. The ratio of the specimen height above the notch to that below it is 2 (cf. Fig. 4.), and an unloaded specimen is shown in Figs. 4 and 5. In the asymmetric specimen, the mode mixity initiated as soon as the crack started propagating. Also, the diameter of the holes was reduced to 3.2mm (1/8'') to make room

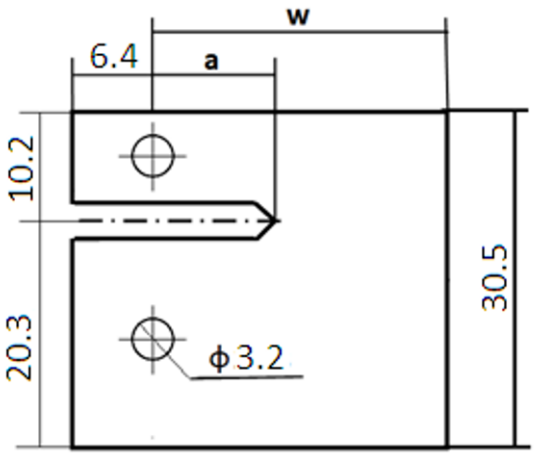

Fig. 4. PMMA asymmetric CT specimens with w=25.4mm (1''), a=12.7mm (0.5''), and the ratio of the specimen height above the notch to that below is 2; B, specimen thickness = 12.7mm (0.5''). (All dimensions in mm).

Fig. 5a. Asymmetric CT specimens with notch and initial crack

for the notch in the narrower arm of the asymmetric geometry. Because of the mode mixity, the crack path was inclined in the direction of the smaller arm (on the top in Fig. 5b). However, the crack path changed direction and became straight (almost perpendicular to the right edge in Fig. 5b) when the crack approached the edge. Additional details on this observation will be discussed in the section on the numerical study and comparisons will be made with the computed results.

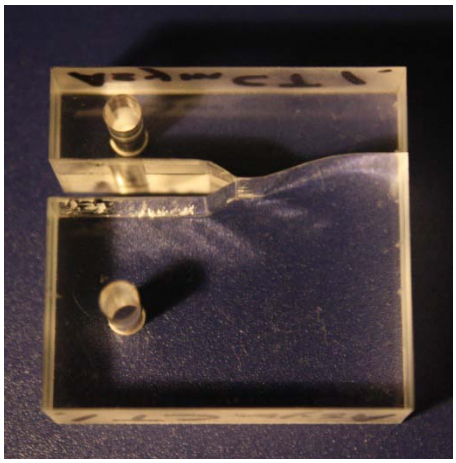

Fig. 5b. Asymmetric CT Specimen with Crack after Test.

Effect of Ratio of Specimen Length / Crack Length on Crack Path Trajectories

The ratio of the specimen length and the initial crack length (w/a) was expected to be important for crack stability. Accordingly, PMMA specimens with different values of w/a were tested. The crack length (a) was varied from 12.7mm (0.5''), to 25.4mm (1''), and 38.1mm (1.5'') while the value of w=101.6 mm (4'') was kept constant; thus w/a equaled 8, 4, and 2.67. The other dimensions were the same as those for the CT specimen. The crack paths are shown in Fig. 6.

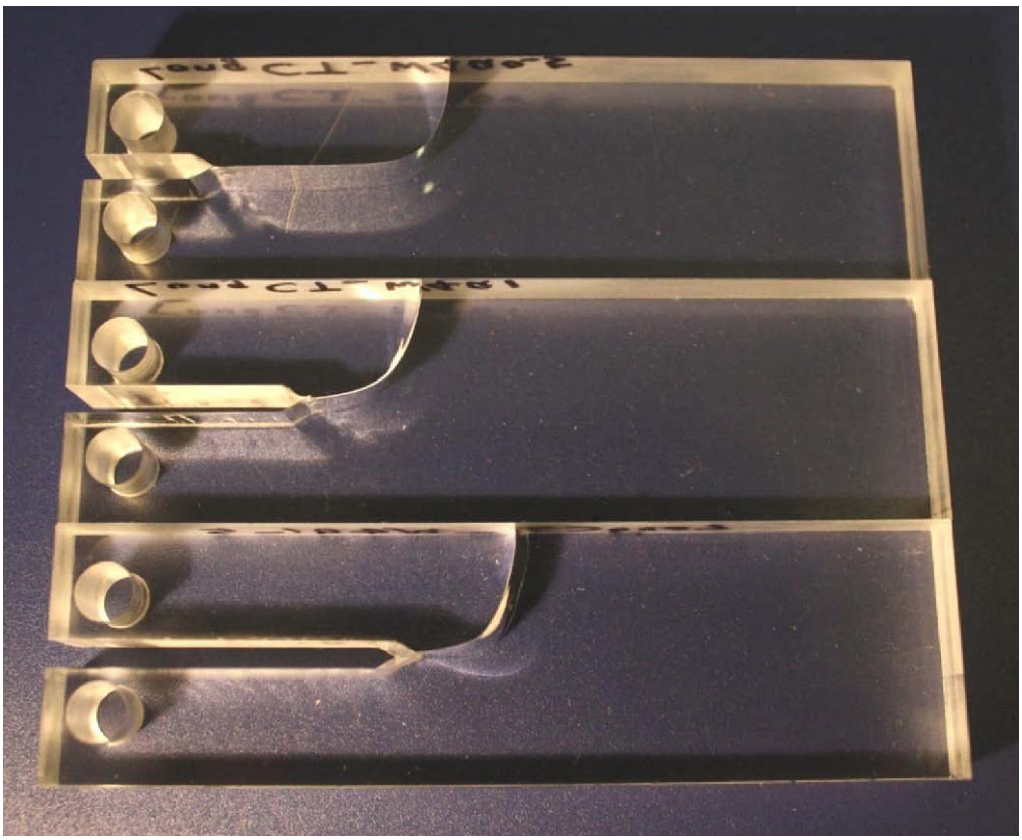

Fig. 6. Trajectories of the crack path of the specimens with different initial crack lengths (From top to bottom: a=12.7mm, 25.4mm, and 38.1mm.)

As the ratio, w/a, was varied from 8, to 4, and 2.67, the crack path became curved and deviated towards one side. The curvatures of the three crack trajectories were almost the same. For specimens with a=25.4mm and 38.1mm, (w/a ≤ 4), the crack curved to one side quickly as soon as propagation started. However, when the initial crack length, a, was 12.7mm (w/a=8), the crack propagated along a straight line for almost 20mm before the deviation started. This suggests that, for small crack lengths, the T-stress is negative and the crack is stable initially. When the crack length increased to some critical value, the T-stress turned positive, destabilizing the crack, and the crack deviated to one side. Additional details will be shown and discussed when test results are compared with those from numerical simulations.

Numerical Studies

Both the finite element (FE) and meshless methods were employed in the numerical studies; the former used the commercial software, ABAQUS™, and the latter our in-house developed computer code.

Finite Element Analysis

The X-FEM (extended finite element method) implemented in ABAQUS™ v.6.9 using 4-node plane strain element, CPE4R, was employed to analyze deformations of the asymmetric CT specimen used in the experimental studies [8, 9]. Assigned boundary conditions simulated as closely as possible those likely to occur in the test configurations. With the loading points shown in Fig. 7a, the following boundary conditions were used in the numerical work.

Load point 1: fixed in x and y directions: u_x= 0, u_y= 0;
Load point 2: fixed in the x-direction and y-displacement prescribed: u_x= 0, u_y= -1 mm.

From tensile tests on PMMA at a strain rate of 0.00014/s and room temperature, Elices and Guinea [10] obtained the following average values: Young's modulus $E = 3000 \pm 30$ MPa, yield limit stress $\sigma_{0.2} = 43.9 \pm 0.7$MPa, rupture stress $\sigma_R = 74.9 \pm 0.2$MPa, and Poisson's ratio $\upsilon = 0.4$; these values were used in our simulations. The maximum principal stress of the damage initiation was set equal to $\sigma_{0.2} = 44$ MPa. Damage evolution was based on fracture energy ($G_{Ic} = G_{IIc} = \frac{{K_{Ic}}^2}{(E/(1-\upsilon^2))} = 312.2\, J/m^2$), linear softening, and mixed mode behavior of power law (α=1) [10]. X-FEM results are show in Figure 7b and will be discussed after meshless methods are introduced.

Analysis of the Problem by the SSPH Method

Meshless methods were introduced in 1970's, and include the Smooth Particle Hydrodynamics (SPH) method [11], Element-Free Galerkin method (EFGM) [12-14], Reproducing Kernel Particle Method (RKPM) [15], Meshless Local Petrov-Galerkin (MLPG) [16], Modified Smoothed Particle Hydrodynamics (MSPH) [17, 18] and Symmetric Smoothed Particle Hydrodynamics (SSPH) [19, 20]. Like the FE and the boundary element methods, meshless methods are used to find an approximate solution of an initial-boundary-value problem with the difference that no element connectivity is needed in a meshless method. Various meshless methods differ in the construction of basis functions for the trial solution.

The EFGM [12-14] has been used to study linear elastic fracture mechanics (LEFM) problems and uses basis functions found by the moving least squares (MLS) method. However, it employs a background mesh to numerically evaluate various integrals appearing in the weak formulation of the problem and thus is not truly meshless. The enriched basis functions [21] are used to capture the stress singularity near a crack-tip without having a very fine distribution of particles (nodes) there. The computational efficiency can be improved by using an appropriate weight or test function [22] and basis functions that better capture singularity of fields near the crack tip [23]. Advantages of the SSPH method are that spatial derivatives of the trial solution are computed without differentiating the basis functions, and the stiffness matrix is symmetric. Our implementation of the SSPH method does not have the enriching terms to capture the stress singularity. We thus use a fine particle distribution around the crack tip. Additional details of the numerical scheme are provided in [24] where results for the CT specimen are also included.

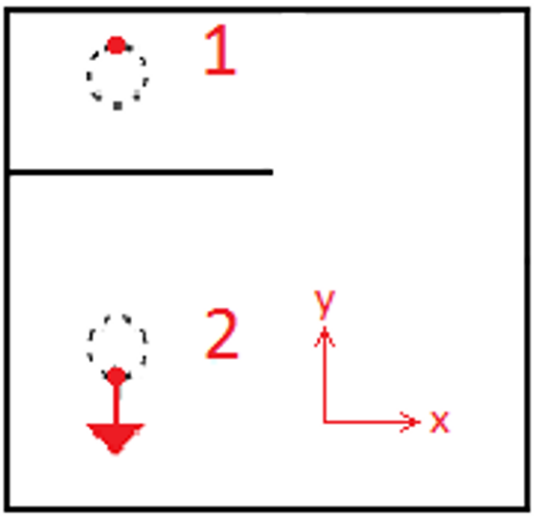

Fig. 7a. Boundary conditions for the asymmetric CT specimen used while analyzing deformations with the commercial software ABAQUS™

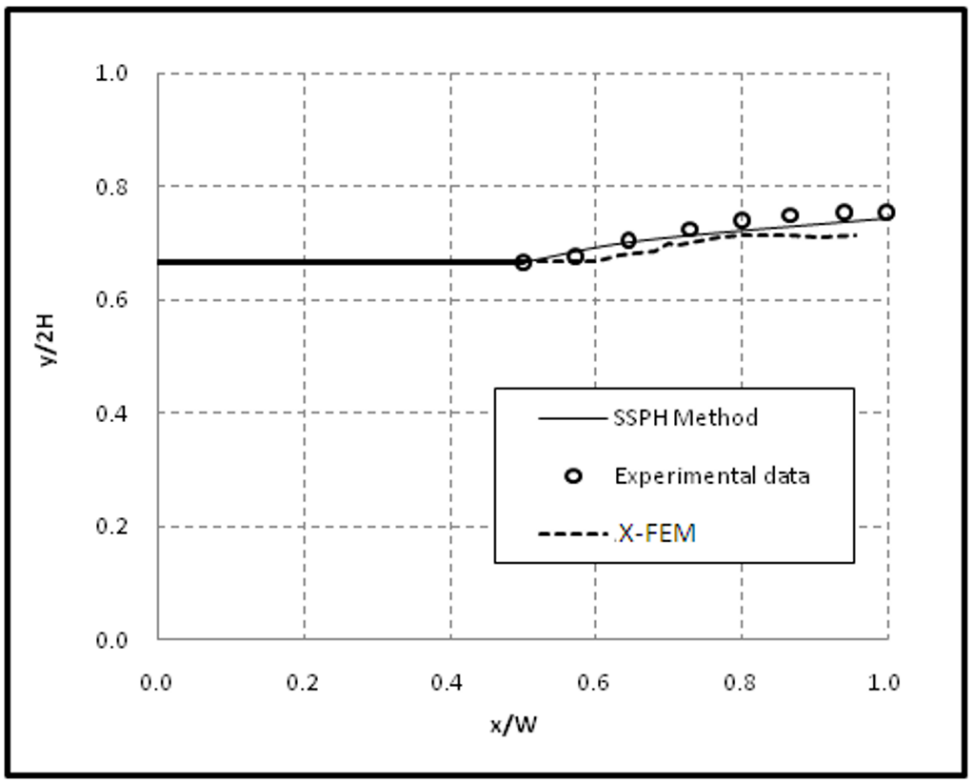

Fig. 7b. Comparison of computed and experimental crack trajectories for an asymmetric CT specimen [The curve denoted by "SSPH Method" will be dicussed in the next section.]

Analysis of deformations of the Double edge notched (DEN) specimen by the SSPH Method

Since the T-stress is expected to play a significant role in the analysis of the crack problem, we first describe results for the mode-I problem obtained by the SSPH method. Deformations of the standard DEN specimen with H=3mm, B=1mm, the crack length ratio (a/B) = 0.2, E = 70GPa and $\nu = 0.3$ have been analyzed. The specimen is subjected to a uniform axial traction S as shown in Fig. 8. Because the specimen geometry and the boundary conditions are symmetric about the x_2-axis, deformations of only the right-half of the specimen are studied. The

analytical expressions for the stress field near the crack-tip are [25]:

$$\begin{bmatrix} \sigma_{11} & \sigma_{12} \\ \sigma_{12} & \sigma_{22} \end{bmatrix} = \frac{K_I}{\sqrt{2\pi r}} \cos(\frac{\theta}{2}) \begin{bmatrix} 1-\sin(\frac{\theta}{2})\sin(\frac{3\theta}{2}) & \sin(\frac{\theta}{2})\sin(\frac{3\theta}{2}) \\ \sin(\frac{\theta}{2})\sin(\frac{3\theta}{2}) & 1+\sin(\frac{\theta}{2})\sin(\frac{3\theta}{2}) \end{bmatrix} + \begin{bmatrix} T & 0 \\ 0 & 0 \end{bmatrix} + O(\sqrt{r}) \quad (1)$$

where (r,θ) are the cylindrical coordinates of a point with the origin located at the crack tip. From Eq. (1), the T-stress along the crack tip, obtained by setting $\theta = 0$, is given by

$$T = \sigma_{11} - \sigma_{22} \quad (2)$$

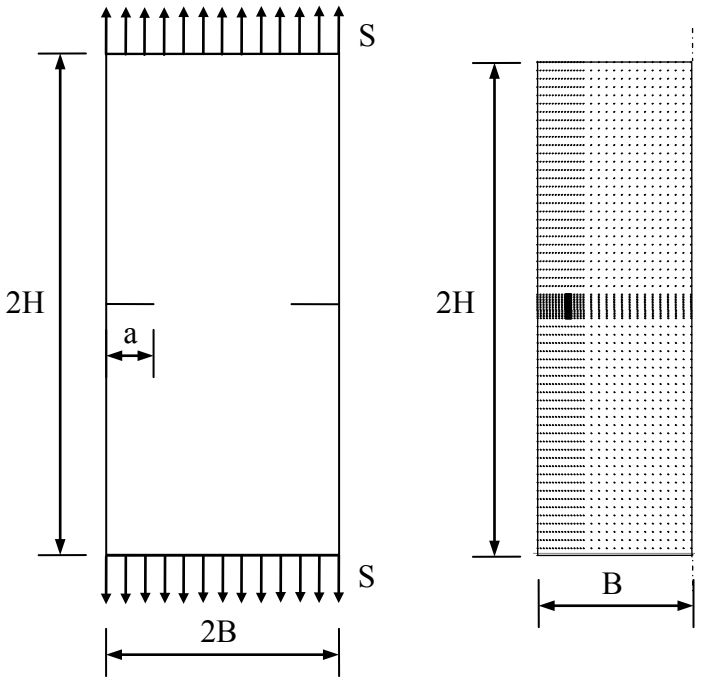

Fig. 8. Double edge notched (DEN) specimen and particles distribution of half model

The computed value, -0.501S, of the T-stress agrees well with of the -0.508S obtained by Kfouri [26].

Analysis of deformations of the Double Cantilever Beam (DCB) specimen by the SSPH Method

The crack trajectories computed by the SSPH method for the DCB specimen shown in Fig. 9 were compared with those found experimentally. Dimensions and material properties for the DCB specimen are: length, $W = 25.4mm$, $2H = 30.5mm$, $a = 12.7mm$, $E = 3.10$ GPa and $\upsilon = 0.35$. A plane strain state of deformation was assumed to prevail in the DCB.

We employed the crack initiation criterion used by Erdogan [27], i.e., a crack initiates when the maximum principal tensile stress reaches a critical value and it propagates in the direction of the eigenvector of this stress. In cylindrical coordinates with the origin at the crack-tip, the stress fields near the crack-tip are [27]

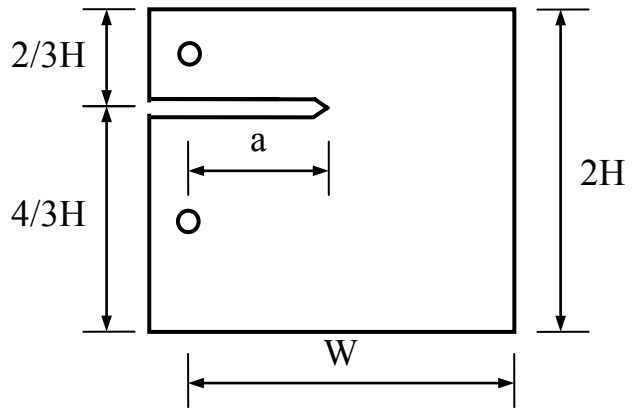

Fig. 9 Double cantilever beam specimen

$$\sigma_{rr}=\frac{1}{\sqrt{2\pi r}}\cos\frac{\theta}{2}\left[K_I\left(1+\sin^2\frac{\theta}{2}\right)+K_{II}\left(\frac{3}{2}\sin\theta-2\tan\frac{\theta}{2}\right)\right]+T\cos^2\theta \tag{3}$$

$$\sigma_{\theta\theta}=\frac{1}{\sqrt{2\pi r}}\cos\frac{\theta}{2}\left[K_I\cos^2\frac{\theta}{2}-\frac{3}{2}K_{II}\sin\theta\right]+T\sin^2\theta \tag{4}$$

$$\sigma_{r\theta}=\frac{1}{\sqrt{2\pi r}}\cos\frac{\theta}{2}\left[K_I\sin\theta+K_{II}(3\cos\theta-1)\right]+T\sin^2\theta \tag{5}$$

where σ_{rr}, $\sigma_{\theta\theta}$ and $\sigma_{r\theta}$ are, respectively, the radial, the circumferential and the shear stresses, K_I and K_{II} are the Mode I and the Mode II stress intensity factors, respectively, and T is the non-singular axial stress. The crack propagation angle θ_0 is found from $\frac{\partial\sigma_{\theta\theta}}{\partial\theta}=0$ or equivalently from

$$\left[K_I\sin\theta_0+K_{II}(3\cos\theta_0-1)\right]-\frac{16T\sqrt{2\pi r_c}}{3}\sin\frac{\theta_0}{2}\cos\theta_0=0 \tag{6}$$

Once the crack initiation criterion has been met, the crack is propagated through the distance 0.02a . Thus the crack propagation analysis may be summarized as follows:

Step1. The displacement, strain and stress fields are determined by using the SSPH method.

Step2. The SIFs are evaluated using the interaction integral based on the results of step1.

Step3. The crack propagation angle θ_0 is determined from Eq. (6).

Step4. The crack is advanced by 0.02a in the direction that makes the angle θ_0 with the horizontal axis.

Step5. Repeat steps1 through 4 until the desired load has been applied on the end faces of the specimen.

In Fig. 7b, we have compared the computed crack path with that found experimentally; and it is clear that the two crack trajectories agree well with each other.

Conclusions

The compact tension PMMA specimens were tested in mode I with a displacement rate of 10 mm/min, and the value of K_{Ic} was found to be 1.056 ± 0.029 MPa$\sqrt{m}$. A set of asymmetric DCB (modified CT) specimens, with the notch and the initial crack not located along the specimen center line, were tested with the goal of investigating crack trajectory deviations due to the mode mixity introduced at the beginning of the crack propagation. Referring to Figs. 4 and 6, the crack first propagated in the lengthwise direction of the specimen, then, briefly, in a transverse direction, followed by the lengthwise direction, and finally nearly perpendicular to the long edge of the specimen. Direction changes in the crack trajectory may be attributed sign switches in the T-stress.

The effect of the specimen length to the initial crack length ratio, w/a, was also studied by testing the modified CT specimens with w/a = 8, 4 and 2.67. For the modified CT specimen with w/a ≤ 4, the crack deviated quickly when propagation started. However, for the specimen with w/a = 8, the crack propagated in a straight line for almost 20 mm before it deviated. These results are in qualitative agreement with those of Aliha and Ayatollahi determined from mixed-mode tests on semi-circular beam specimens of PMMA [1].

Deformations of pre-notched specimens were also analyzed by the X-FEM implemented in the commercial software, ABAQUS™, and the meshless SSPH method implemented in the in-house developed computer software. As should be clear from the results plotted in Fig. 7, the crack path predicted by the SSPH method is in better agreement with that found experimentally than the crack path computed using the X-FEM. However, this needs to be checked for several test configurations before the superiority of the SSPH method over the X-FEM can be ascertained.

Acknowledgements

The authors are grateful for support from the National Science Foundation (NSF/CMMI Award No. 0826143). YG would also like to thank the China Scholarship Council for partial support during this work.

References

1. Aliha, M.R.M., Ayatollahi, M. R., *Geometry effects on fracture behaviour of polymethyl methacrylate.* Materials Science and Engineering A-Structural Material Properties Microstructure and Processing, 2010 **527**(3): p. 526-530.
2. Ayatollahi, M.R., Aliha, M. R. M., Hassani, M. M. , *Mixed mode brittle fracture in PMMA - An experimental study using SCB specimens* Materials Science and Engineering A-Structural Materials Properties Microstructure and Processing, 2006 **417**(1-2): p. 348-356.
3. Smith, D.J., Ayatollahi, M. R., Pavier, M. J., *The role of T-stress in brittle fracture for linear elastic materials under mixed-mode loading.* Fatigue Fract Engng Mater Struct, 2001 **24**: p. 137–150.
4. Mahajan, R.V., and Ravi-Chandar, K., *An experimental investigation of mixed-mode fracture.* International Journal of Fracture, 1989 **41**: p. 235-252.
5. Gomez, F.J., Elices, M., Planas, J., *The cohesive crack concept: application to PMMA at -60 oC.* Engineering Fracture Mechanics, 2005 **72**(8): p. 1268-1285
6. Williams, M.L., *On stress distribution at base of stationary crack.* American Society of Mechanical Engineers -- Transactions -- Journal of Applied Mechanics, 1957 **24**(1): p. 109-114.
7. ASTM, *D5045 - 99(2007)e1 Standard Test Methods for Plane-Strain Fracture Toughness and Strain Energy Release Rate of Plastic Materials*. 2007, ASTM International: West Conshohocken, PA.
8. Hibbitt, K., Sorensen, Inc., *ABAQUS/standard user's manual, v.6.9*. 2009, Pawtucket, Rhode Island.
9. Giner, E., Sukumar, N., Tarancon, J. E., Fuenmayor, F. J., *An ABAQUS implementation of the extended finite element method.* Engineering Fracture Mechancs, 2009 **76**(3): p. 347-368.
10. Elices, M., Guinea, G. V., *The cohesive zone model: advantages, limitations, and challenges.* Engineering Fracture Mechanics, 2002 **69**(2): p. 137-163.
11. Lucy, L.B., *A numerical approach to the testing of the fission hypothesis.* Astron J, 1977 **82**: p. 1013–1024.

12. Belytschko, T., Lu, Y. Y. and Gu, L. , *Element-free Galerkin methods.* International Journal for Numerical Methods in Engineering, 1994 **37**: p. 229-256.
13. Lu, Y.Y.B., T., and Gu, L. , *A new implementation of the element free Galerkin method.* Comp. Meth. Appl. Mech. Engng 1994 **113**: p. 397-414.
14. Lu, Y.Y., Belytschko, T., and Gu, L. , *Crack propagation by element-free Galerkin methods.* Engng Frac. Mech. , 1995 **51**(2): p. 295-315.
15. Liu, W.K., Jun, S., Zhang, Y. F., *Reproducing kernel particle methods.* Int J Num Meth Fl 1995 **20**(1081–1106).
16. Atluri, S.N., and Zhu, T. , *A new meshless local Petrov-Galerkin (MLPG) approach in computational mechanics.* Computational Mechanics 1998 **22**: p. 117-127.
17. Zhang, G.M., Batra, R. C. , *Modified smoothed particle hydrodynamics method and its application to transient problems.* Comput. Mech., 2004 **34**: p. 137–146.
18. Batra, R.C., Zhang, G. M., *Analysis of adiabatic shear bands in elasto-thermo- viscoplastic materials by modified smoothed particle hydrodynamics (MSPH) method.* JComput Phys 2004 **201**: p. 172–190.
19. Batra, R.C., and Zhang, G. M, *SSPH basis functions for meshless methods and comparison of solutions with strong and weak formulations.* Computational Mechanics 2008 **41**: p. 527-545.
20. Zhang, G.M., and Batra, R. C., *Symmetric smoothed particle hydrodynamics (SSPH) method and its application to elastic problems.* Computational Mechanics 2009 **43**: p. 321-340.
21. Fleming, M., Chu, Y., Moran, B., and Belytschko, T. , *Enriched element-free Galerkin methods for crack tip fields.* International Journal for Numerical Methods in Engineering 1997 **40**: p. 1483-1504.
22. Rao, B.N., Rahman, S., *An efficient meshless method for fracture analysis of cracks.* Computational Mechanics 2000 **26**: p. 398-408.
23. Hildebrand, G., *Fracture analysis using an enriched meshless method.* Meccanica DOI 10.1007/s11012-008-9189-4, 2009.
24. Tsai, C.L., Guan, Y. L., Batra, R. C., Ohanehi,D. C., Dillard, J. G., Nicoli, E., Dillard, D. A., *Coupled experimental & computational analysis of fracture of PMMA blocks under mixed mode loading.* Experimental Mechanics, 2010 ([under preparation]).
25. Willams, M.L., *On the stress distribution at the base of a stationary crack.* J Appl Mech 1957 **24**: p. 109-114.
26. Kfouri, A.P., *Some evaluations of elastic T -term using Eshelby's method.* International Journal of Fracture, 1986 **30**(4): p. 301-315.
27. Erdogan, F., and Sih, G. C. , *On the crack extension in constraint effects in plates under plane loading and transverse shear.* Trans. ASME, J. Bas. Engng, 1963 **85 D**: p. 525–527.